THEORETICAL NOTES

Note 190

October 1973

SENSITIVITY OF SELF-CONSISTENT HIGH-ALTITUDE ELECTROMAGNETIC PULSE CALCULATIONS TO PREIONIZATION AND IMPROVED SOURCE AND IONIZATION MODELS

G. H. Canavan, Maj, USAF
J. E. Brau, Capt, USAF
L. A. Wittwer, Capt, USAF

Air Force Weapons Laboratory
Kirtland AFB, New Mexico

ABSTRACT

The Air Force Weapons Laboratory CHEMP code for self-consistent calculations of high-altitude electromagnetic pulse is used here to assess the energetic consequences of self-consistency, with particular attention to the alteration of the radiated electromagnetic pulse. Parametric studies indicate the sensitivity of the radiated fields to gamma spectrum, angular distribution of Compton electrons, scattering, cascading, and source region conductivity. The latter point is elaborated on through predictions of the reduction of radiated fields by small amounts of precursor ionization in the source region.

CONTENTS

ILLUSTRATIONS

ILLUSTRATIONS (cont'd)

TABLES

SECTION I

INTRODUCTION

The appendix assesses the violation of energy conservation caused by the nonself-consistent treatment of the interaction between currents and fields in the electromagnetic pulse (EMP) (ref. 1) algorithm. This report complements that discussion with an indication of the reduction of the radiated fields by self-consistency, uncertainties in the electron mobility, and cascading effects. This report summarizes the results obtained above and evaluates their sensitivity to initial distribution and small angle scattering of the Compton sources and to ionization remaining in the source region from previous bursts.

SECTION II

SELF-CONSISTENCY

The effect of self-consistency was evaluated through calculations with CHEMP, an Air Force Weapons Laboratory (AFWL) electron pushing code (ref. 2) capable of either self-consistent, CHEMP(S), or nonself-consistent, CHEMP(N), modes of operation. When run in the latter, the CHEMP(N) algorithm essentially reduces to that of reference 1, and as figure 1 shows, reproduces the predictions of the EMP code described in the appendix to within a residual error which may be attributed to differences in numerical techniques. Figure 2 shows the alteration of the (proper) time dependent EMP field at the ground and at the altitude of maximum field when CHEMP is run in the self-consistent mode for a 100-km burst with gamma yield of 0.25 KT. While the fields are altered but little at early times, the peak fields both on the ground and at altitude are reduced by 25 percent--a correction which grows with time in the saturated tails of the pulses. The combination of the lower peak and truncated pulse length reduces the total fluence in the EMP pulse at the ground by roughly a factor of three for this burst.

Figures 3 through 5 show how self-consistency affects the fraction of the energy initially deposited in Comptons which is in radiated EMP f_r, resistively dissipated f_d, in longitudinal fields f_l, in kinetic energy of the primaries f_k, and in secondary ionization f_i (ref. 2) at proper times of 2, 4, and 5.8 shakes, respectively. Figure 3 shows that up to the time of peak field, the dominant effect of self-consistency is the reduction of f_k to account for the transfer of energy from primary kinetic energy to EMP. This deceleration of the primaries is reflected in a reduced EMP fluence transmitted through the bottom of the 40 to 30 km generation zones and consequently in a reduction in the energy resistively removed from the EMP fields in the 30 to 20 km dissipative zone. These patterns are repeated in the 4-shake curves of figure 4 where the somewhat diffuse boundary between the generation and dissipation regions has shifted to higher altitude as a result of the growth of ionization below 40 km. Though the buildup of currents at altitude lead to appreciable efficiencies of conversion

to EMP at 40 km, most of the energy is dissipated at 40 to 30 km with an ever decreasing fraction reaching the ground. At 5.8 shakes, figure 5 shows that the 50-percent violation of energy conservation in the CHEMP(N) calculation is corrected by CHEMP(S) (for which the obvious energy identity $1 = f_k + f_d + f_i + f_r + f_l$ is satisfied to better than 0.3 percent at all times) through a 30-percent reduction in f_k, a similar reduction in f_r at altitude, and a consequent 50-percent reduction of f_d below. The factor-of-three reduction in f_r at the ground is in accord with the estimate above based on inspection of figure 2.

Figure 6 shows how the time dependence of the fields on the ground and at altitude vary with yield for a 100-km burst. With increasing yield the field peaks out earlier at a slightly higher level, then decreases more rapidly during saturation. Figure 7 contrasts the dashed CHEMP(S) peak fields with the solid CHEMP(N) fields in order to demonstrate the increasing importance of self-consistency with yield.

The calculations from which the above conclusions were made were for only one nonoptimal geometry and with a simplified source and ionization model. It was felt that such simplifications would not seriously affect the phenomenon being studied, i.e., the effects of self-consistency, height of burst, and yield. Because of the simplifications, however, no interpretation can be made as to the expected absolute magnitudes of EMP fields.

SECTION III

IMPROVEMENTS IN SOURCES

The EMP physical model has undergone considerable improvement over the simplified model used in generating figures 1 through 7. The gamma pulses used in these figures, plus figure 8, were proportional to a function. $f(t) \propto e^{-A/t-Bt}$ where t is in seconds, $A = 10^{-9}$, and $B = 10^{7}$. Figures 11, 13, 14, and 15 used a pulse characterized by $A = 2 \times 10^{-8}$ and $B = 2 \times 10^{8}$. This pulse was used for comparison with calculations by Dr. Cullen Crain (ref. 4). Figure 10 was with a pulse $f(t) \propto \exp(8 \times 10^{8}(t-t_0))/(1 + 5.71 \exp(9.4 \times 10^{8}(t-t_0)))$ for comparison with the worst case geometry (WCG) result of Mission Research Corporation (MRC) (ref. 4). Finally, figure 17 used a pulse with $A = 4.0 \times 10^{-8}$ and $B = 4.4 \times 10^{7}$ to examine the effects of a wider pulse. The rise time is defined as α when the rise of the gamma pulse is characterized by $e^{\alpha t}$. Unfortunately, except for figure 10, the pulses used by AFWL for the calculations presented here are not clearly characterized by a rise time. Thus, the rise of the EMP fields must be interpreted with some care.

A more significant feature is the use here of the simple approximation introduced in reference 1 that upon its first scattering each 1.5-MeV gamma is replaced by a single forward-directed 0.75-MeV Compton electron. Figure 8 is a plot of the time dependence of the field on the ground directly below a 0.25-KT long pulse source of 1.5-MeV gammas at 100 km. Curve A shows that the peak field from the one-particle model is larger by more than a factor of two than those in curves B and D in which the scattered gamma was replaced by 16 Compton electrons distributed in a 4 x 4 array over polar and azimuthal angles with respect to the direction of the incident gamma according to the differential Klein-Nishina scattering probability, a prescription formalized by Longmire in reference 5. Curves B and D reflect different statistical weighting of the particles. This distribution of the sources degrades their coherence which inevitably leads to a reduction in their radiating efficiency and hence the fields observed on the ground. Changes produced by using N x N arrays with $N > 4$ do not produce effects so dramatic as those seen in going from 1 x 1 to 4 x 4 (ref. 5) which is fortunate in that the storage and time required for computer calculations with CHEMP increases as N^2.

The assumption of a monoenergic gamma spectrum, which is often made for simplicity and to avoid poorly characterized weapon outputs, is not without consequences. Curve C of figure 8 shows the 50 percent increase in the peak field from a calculation which assumes 3-MeV gammas rather than the 1.5-MeV gammas of curves B and D. Curve F shows, however, that a further increase to 5-MeV gammas produces no further increase in the fields. Sensitivity to monoenergicity was tested by a calculation in which the gammas were distributed in energy fractions 0.25/0.5/0.25 over 0.75/1.5/3.0 MeV with results which differ from B and D by less than they differ from each other.

A further omission in the treatment of sources is the neglect of the degradation of the Compton currents by small-angle scattering. Curve E of figure 8 shows that small-angle scattering, included via the "obliquity model" of Longmire (ref. 5), results in another x 2 reduction in the peak fields directly below a 0.25-KT long pulse of 1.5-MeV gammas over and above that from the 4 x 4 angular distribution of curve B. Since the obliquity model currents have been shown by Karzas (ref. 6) to be in agreement with the detailed Monte-Carlo scattering treatment by Knutson (ref. 7) over the time interval of interest here, it is felt that this x 2 reduction cited above is a reasonable estimate of the effects of nuclear scattering. Recently, AFWL (ref. 8) has carried out new Monte-Carlo calculations to determine the effects of nuclear scattering using both the Karzas high-frequency approximation (ref. 9) and the Crain particle (ref. 10) formalism. The different formulations were shown to be equivalent and upheld the validity of the MRC obliquity model for electron energies of interest in agreement with the original Karzas note (ref. 6).

SECTION IV

IONIZATION LAG

One might assume that for every ionizing collision by a Compton electron, 86 eV of energy were lost with the immediate gain of 2.5 ions. In fact, there is a time lag between the initial ionization event and the realization of the net ionization. This problem was first approximately treated by Longmire (ref. 11). The fractional increase in net ionization with time from a 1-MeV Compton ionization event at 30 km is shown in figure 9 as curve A. This model was then improved by Longmire (ref. 12) using a more exact Boltzman treatment. The result, curve B, is not significantly different from the earlier model. The Air Force Weapons Laboratory then developed a Boltzman code to first reproduce the Longmire calculations, curve C, and then used an improved form for the electron energy distributions taken from high-energy electron energy loss calculations in air (ref. 13). This result is curve D. Curve D indicates that the ionization increases slightly faster than predicted by Longmire. However, the calculations leading to D resulted in a net ion per 39 eV rather than 32.5 as generally accepted and as found in the Longmire calculation. This discrepancy has yet not been resolved. At present, AFWL is using a model represented by curve E. The effect of using an ionization lag model is to slightly increase the field strengths.

The "standard" calculation is currently based on the CHEMP algorithm of reference 2 modified by a swarm treatment (ref. 14) of secondary electrons, a 4 x 4 initial angular distribution of Comptons (ref. 5), an obliquity model (ref. 5) for the treatment of small angle scattering, and an ionization lag model. Since the physical processes treated in this standard calculation with the exception of the ionization lag model are the same as those included in the independently developed CHAP code of MRC (ref. 5), it is not surprising (but is a relief) to see the excellent agreement of figure 10 between CHAP (ref. 4) and CHEMP 4 x 4 calculations of fields on the ground in the WCG from a 25-KT, 8/shake rise source of 1.5-MeV gammas at 250 km. These pulses, incidentally, represent the largest EMP field, roughly 30 kilovolt/meter for 1 shake, found by either group in the WCG. These calculations, however, are not really worst

case because ionization lag was omitted. The WCG is a ray which descends from the burst at 60 degrees from the vertical, perpendicular to a maximum continental geomagnitic field of 0.6 gauss. Along this WCG the currents in the source region and hence the fields on the ground scale on the ratio of gamma yield Y to the square of the distance R between the burst point and the source region. Since in the WCG, R is proportional to the burst altitude Z, WCG bursts are most properly characterized by Y/Z^2, and the maximum EMP in figure 10 could as well be regarded as arising from a roughly 1.5-KT source at 100 km.

Some indication of how the WCG fields vary with yield is provided by figure 11, which shows EMP on the ground from 1, 10, and 100-KT fast pulses of 1.5 MeV gammas at 250 km. With increasing yield the field peaks out earlier at a higher level and then decreases more rapidly during saturation. The first column of table 1 shows that this occurs in such a manner that the energy fluence $F = \int dt\ cE^2/4\pi$ and impulse $I = \int dt\ E$ are relatively insensitive to yield Y, and hence Y/Z^2, in the WCG. The transforms of the fields in figure 12 show further that in the 1 to 10 MHz region the spectra of the three yields differ very little from each other. The secondary peaks at high frequencies are unphysical--they merely indicate the point above which the results are model dependent.

The peak field of 1.4 electrostatic units (esu) from the 100-KT burst of figure 11 would seem to contradict the earlier assertion that the 1-esu peak from the 25-KT burst of figure 10 represents the maximum EMP expected in the WCG without ionization lag. Figure 11, however, uses a pulse with a larger effective rise time which allows the fields to attain slightly higher values before saturating than the 8/shake rise of figure 10. Thus, the citation of figure 10 of this report as the maximum WCG EMP is predicted on alphas of roughly 8/shakes being the maximum attainable at large yields.

Table 1

IMPULSE AND ENERGY FLUENCE FOR VARIOUS PULSES

Pulse Description	1 KT	10 KT	100 KT
Fast pulse without preionization			
Impulse (esu-sec)	3.0×10^{-8}	2.9×10^{-8}	2.4×10^{-8}
Energy fluence (mj/m^2)	24	33	30
Fast pulse with preionization			
Impulse (esu-sec)	1.1×10^{-8}	1.8×10^{-8}	2.0×10^{-8}
Energy fluence (mj/m^2)	4	12	17
Medium pulse with preionization			
Impulse (esu-sec)	1.2×10^{-8}	2.3×10^{-8}	2.2×10^{-8}
Energy fluence (mj/m^2)	3	14	19

SECTION V

PREIONIZATION

In response to estimates by Crain (ref. 3) of the reduction of the fields from a burst due to ionization remaining in the source region from previous bursts, the exploratory 1 x 1 calculations shown in figure 13 of the reduction of the fields on the ground directly below 0.25, 2.5, and 25 KT short pulses of 1.5-MeV gammas from 100 km by the ionization left in the source region by a precursor burst of 0.03 KT of 1.0-MeV gammas at the same point a few microseconds earlier were performed. The effect was quite dramatic, with the field from the preionized 25-KT source being smaller than that from the 0.03-KT precursor, and the field from the preionized 0.25-KT source being essentially eliminated. The reason for this drastic modification is that the fields, which rise to their peak before the buildup of secondary ionization in calculations without preionization, are saturated from the outset with preionization due to conduction currents carried by the electrons left by the precursor. Recall, however, that figure 13 represents an extreme case: straight down perpendicular to a 0.6 gauss field. Figure 14 shows that the alteration is much less for rays tangent to the earth's limb. Here, the correction is only x 2 for 0.25 KT, and much smaller for the larger yields, although they are noticeably smoothed by the precursor.

A more precise evaluation of the effect of preionization is afforded by figure 15 which reports 4 x 4 calculations of the WCG fields at the ground from 1, 10, and 100-KT short pulses of 1.5-MeV gammas preionized by 0.1 KT of 1.5-MeV gammas. The reduction in peak fields is considerable: 0.2, 0.6, and 0.8 esu compared to the peaks of 0.6, 1.1, and 1.4 esu from figure 11 without preionization. Further, the second column of table 1 shows that the pulses no longer have the same I and F. The 100-KT burst has twice the impulse and four times the energy fluence of the 1 KT. Preionization discriminates strongly against the smaller bursts, since they are less able to produce the Compton currents needed to overcome the conduction currents in the precursor ionization. Note that in figure 15 the late time tails are the same for all three yields and virtually identical to that from the 100-KT burst without preionization in figure 11. The

transforms, figure 16, of figure 15 show a x 2 spread in the preionized spectra in the 1 to 10 MHz region consistent with the x 2 spread in impulse in table 1. Only the 1-KT burst is strongly affected in this interval. The dominant effect in all cases is, as expected, a faster roll-off at higher frequencies.

Figures 17 and 18 show that the same qualitative features emerge both temporally and spectrally with a wider gamma pulse, including the asymptotic approach to a common tail, though on a longer time scale. Colume 3 of table 1 shows that the impulse and fluence from the preionized longer pulse are essentially the same as those from the short. It is instructive to proceed through table 1 horizontally as well, noting that for 1-KT, preionization decreases the impulse by 3 and the energy by 6, while for 10 KT the reductions are less than 2 and 3, respectively. For 100 KT the energy is decreased only by two, the impulse being essentially unaltered. In summary, while in the absence of preionization the threat posed is but weakly dependent of yield (or Y/Z^2), with preionization larger yields present more severe environments by factors of two to four.

APPENDIX

ENERGY CONVERSION IN EMP CALCULATIONS

The calculations reported here are based on the equations for the high altitude electromagnetic pulse algorithm (ref. 1) and are performed in order to assess the significance of the nonself-consistent treatment of the fields in early AFWL EMP calculations.

The EMP signal from an exospheric burst is generated by the gamma-produced Compton electrons as they turn in the earth's geomagnetic field. The primary source region is at 60 to 40 km altitude where the air is dense enough to cause significant interaction with the gammas but not dense enough to stop the Comptons before they complete a substantial portion of a cyclotron orbit. Figure 19 shows the (proper) time dependence of the radiated EMP field directly below a Z_b = 100 km burst, at R = 65 km, the altitude at which the field is maximized, at R = 80 km below, and the EMP field transmitted to the ground from a $N_g h\nu$ = 10^{19} erg input pulse of $h\nu$ = 1.5 MeV gammas with a rise time of 1 shake and fall of 10 shakes. The 0.7 MeV Compton electrons are assumed initially to be forward directed and interact with the earth's 0.3 gauss geomagnetic field (perpendicular to motion of gammas and parallel to earth's surface). Table 2 shows the unattenuated gamma energy per unit area passing an altitude $Z = Z_b - R$

$$W_g = N_g h\nu/4\pi R^2 \tag{1}$$

and the gamma energy per unit area converted into Compton electrons of average kinetic energy T = 0.74 MeV via Comption collisions with cross section $\sigma_c = 2.3 \times 10^{-24}$ cm^2 in air of molecular number density $N_a(r)$

$$W_c = T\, N_g \left[1 - \exp\left(-\int_0^R dr N_a(r)\, \sigma_c\right)\right]/4\pi R^2 \tag{2}$$

Of W_c, a portion W_i is used in producing secondary ionization at a rate/cc of $\dot{n}_e$

Table 2

ENERGY FLUENCES AND FRACTIONS AS A FUNCTION OF ALTITUDE

Altitude (km)	W_g (erg/cm^2)	W_c	W_r	W_d	f_c	f_r	f_d
70	8.8×10^4	8.0×10	6.6×10	2.9	0.001	0.82	0.02
60	5.0×10^4	2.1×10^2	3.5×10^2	4.9×10	0.004	1.7	0.08
50	3.2×10^4	5.8×10^2	1.6×10^3	8.6×10^2	0.018	2.7	0.28
40	2.2×10^4	1.6×10^3	2.8×10^3	7.9×10^3	0.075	1.7	0.64
30	1.6×10^4	4.0×10^3	1.2×10^3	1.8×10^4	0.25	0.30	0.78
20	1.2×10^4	5.6×10^3	2.6×10^2	1.5×10^4	0.47	0.044	0.72
10	9.8×10^3	4.8×10^3	1.7×10^2	1.2×10^4	0.49	0.036	0.71
0	8.0×10^3	3.9×10^3	1.4×10^2	9.7×10^3	0.49	0.036	0.71

$$W_i = \int_0^\infty dt \int_0^R dr\, r^2 q \dot{n}_e(r,t)/R^2 \tag{3}$$

with q = 34 ev/ion pair being subtracted from the energy of the primary. Table 2 also displays the EMP fluence passing R

$$W_r = \int_0^\infty dt\, cE^2(R,t)/4\pi \tag{4}$$

and the energy resistively dissipated above R

$$W_d = \int_0^\infty dt \int_0^R dr\, r^2 \sigma(r,t) E^2(r,t)/R^2 \tag{5}$$

using the self-consistently computed conductivity σ. Dropping through the source region, the fractional gamma energy converted into Comptons $f_c = W_c/W_g$ rises to $0.49 \approx T/h\nu$, the fractional energy in the fields $f_r = W_r/W_c$ falls, and the fractional energy dissipated $f_d = W_d/\left(W_i + W_r + W_d\right)$ approaches one.

Figure 20 shows how the fields vary with W_g. Note that $W_r \propto E^2$ exhibits a disturbing secular growth which can be traced to the nonself-consistent neglect of the back reaction of the radiated fields on the Compton sources. This allows the fields at a fixed altitude to scale as $E \propto W_g$ and hence $W_r \propto E^2 \propto W_g^2$ (until the fields are shorted by the anomalously large conduction currents), so that $f_r \propto W_g$ can exceed unity for large yields at high altitudes, violating the obvious energy conservation relationship

$$W_c = W_i + W_r + W_d, \text{ or } 1 = f_i + f_r + f_d \text{ for all } R \qquad (6)$$

Since the reaction of the time dependent fields back on the primaries is neglected, their only energy loss is that due to secondary production, which explains the seemingly paradoxical result that $W_i = W_c$ or $f_i = 1$ in EMP calculations. By contrast, the fraction of the field energy converted to heat by the swarm electrons is well behaved. Since $W_d \propto (\sigma E^2)_{max}$, and $\sigma \propto \mu n_e$, where the electron mobility $\mu \propto E^{-1/2}$ and number density $n_e \propto W_g$, one has $W_d \sim W_g^{5/2}$ and $f_d \sim 1$ for high yields. Note, however, that even with reasonable conversion ratios f_d, W_d can exceed W_c due to the nonconservative excesses of W_r, since

$$W_d = W_r + W_i \; f_d / 1 - f_d = W_c \, f_r + f_i \, f_d / 1 - f_d \qquad (7)$$

can exceed W_c even for $f_d < 1$ when equation (6) is violated.

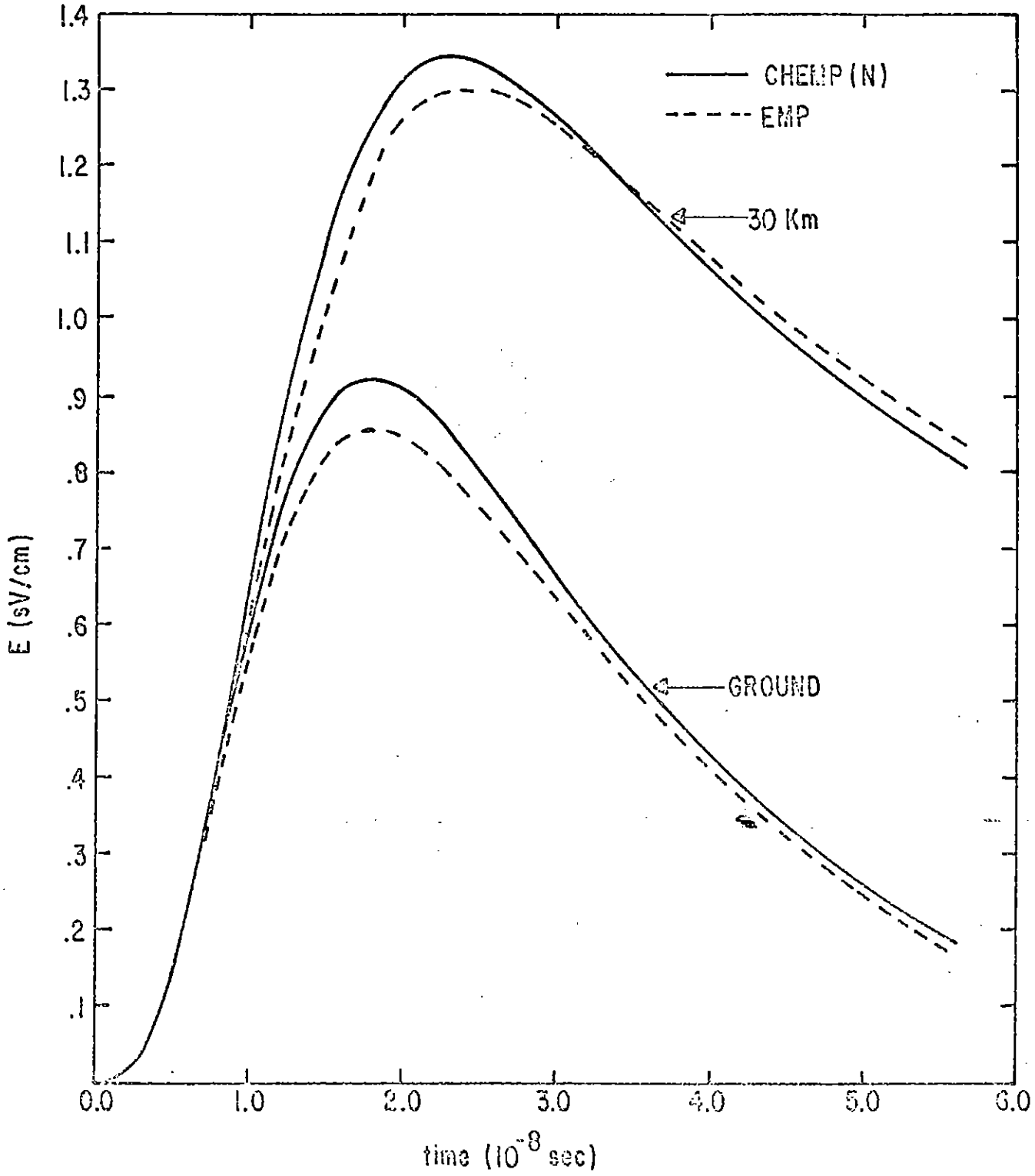

Figure 1. Comparison of the EMP Fields Directly Below 0.25 KT Burst at 100 km for CHEMP(N) and EMP Calculations Using the Algorith of Reference 1

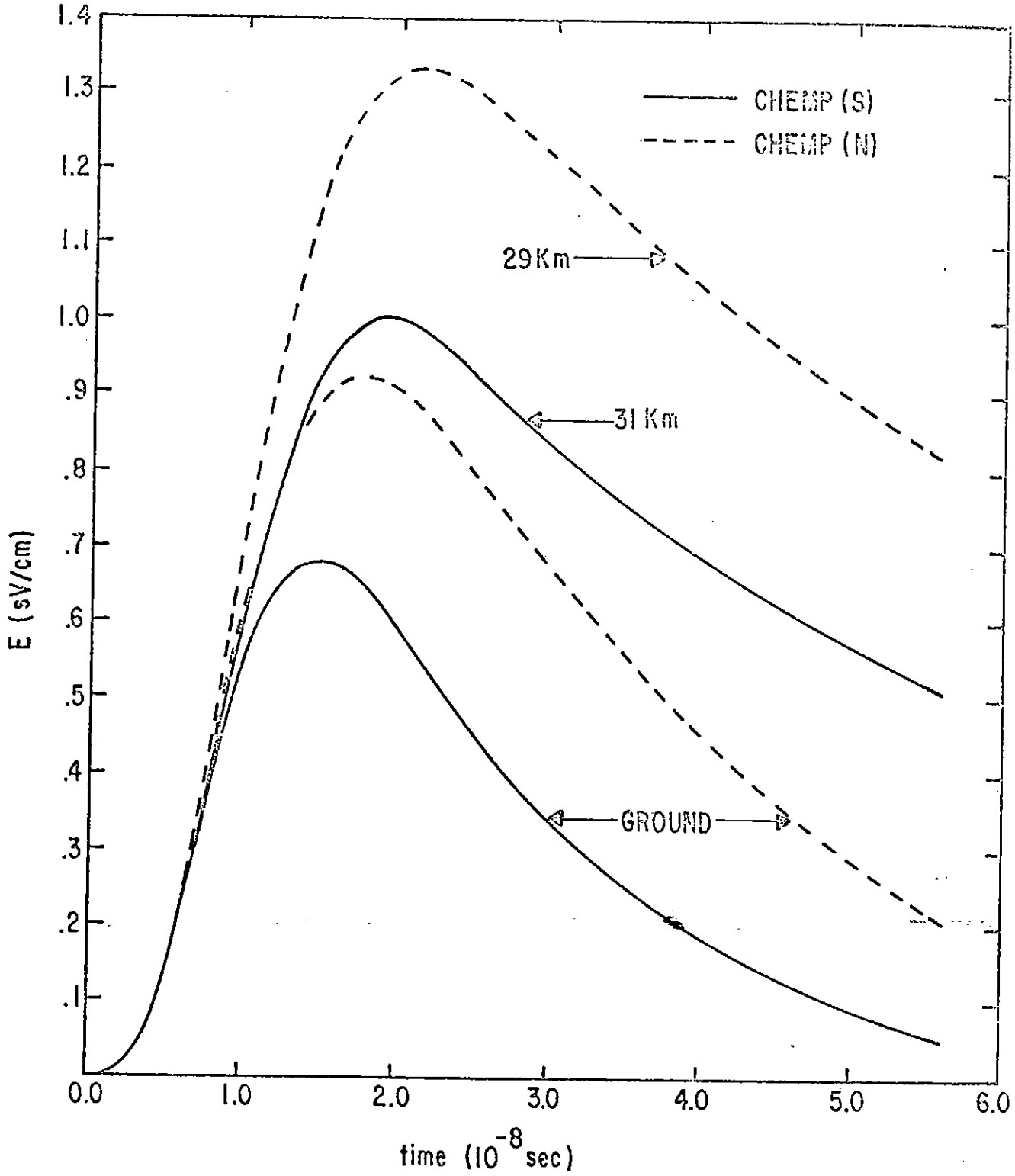

Figure 2. EMP Fields at the Ground and at the Altitude of Maximum Field Directly Below a 0.25 KT Burst at 100 km from CHEMP(S) and (N) Calculations

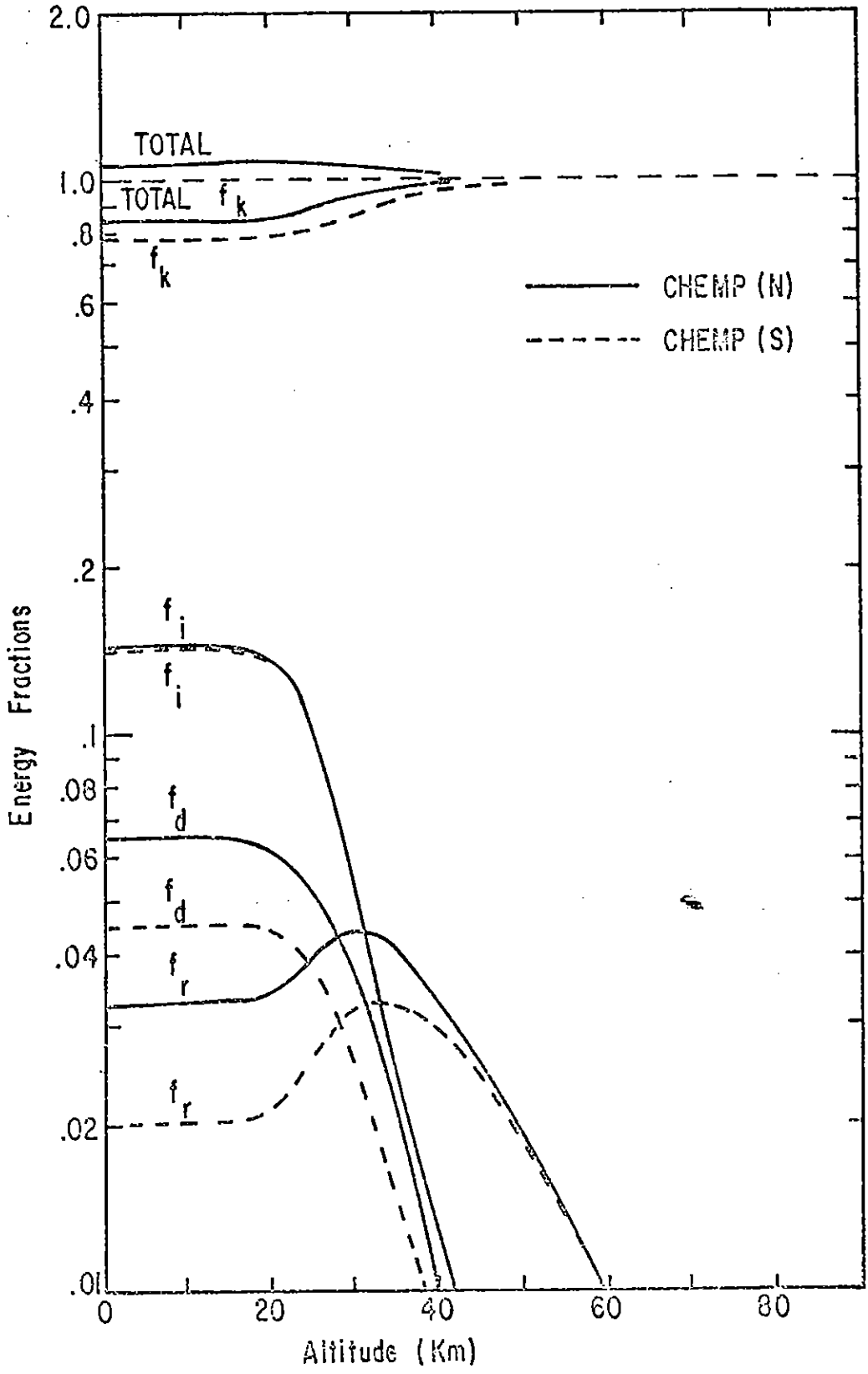

Figure 3. Energy Fractions at 2.0×10^{-8} sec

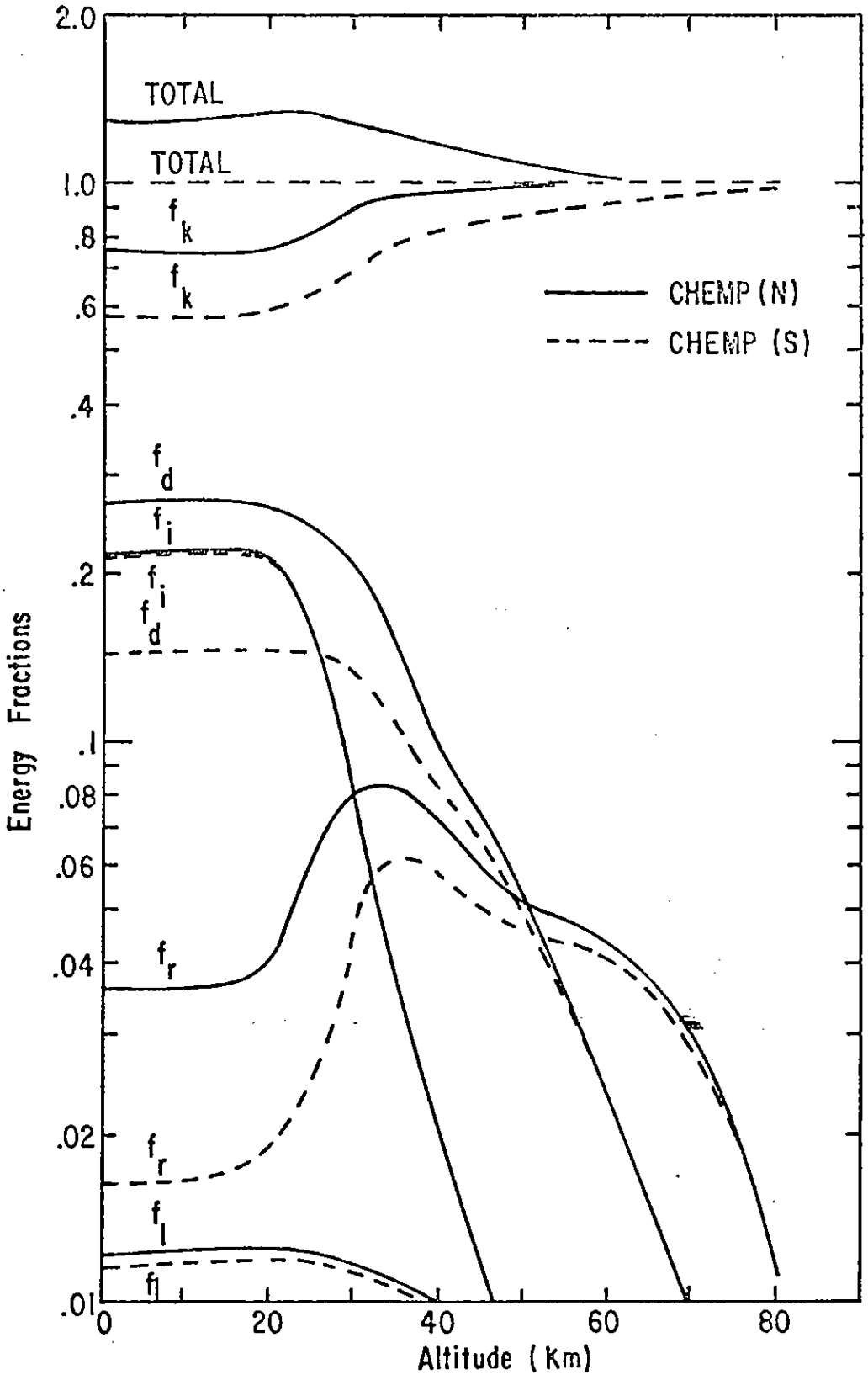

Figure 4. Energy Fractions at 4.0×10^{-8} sec

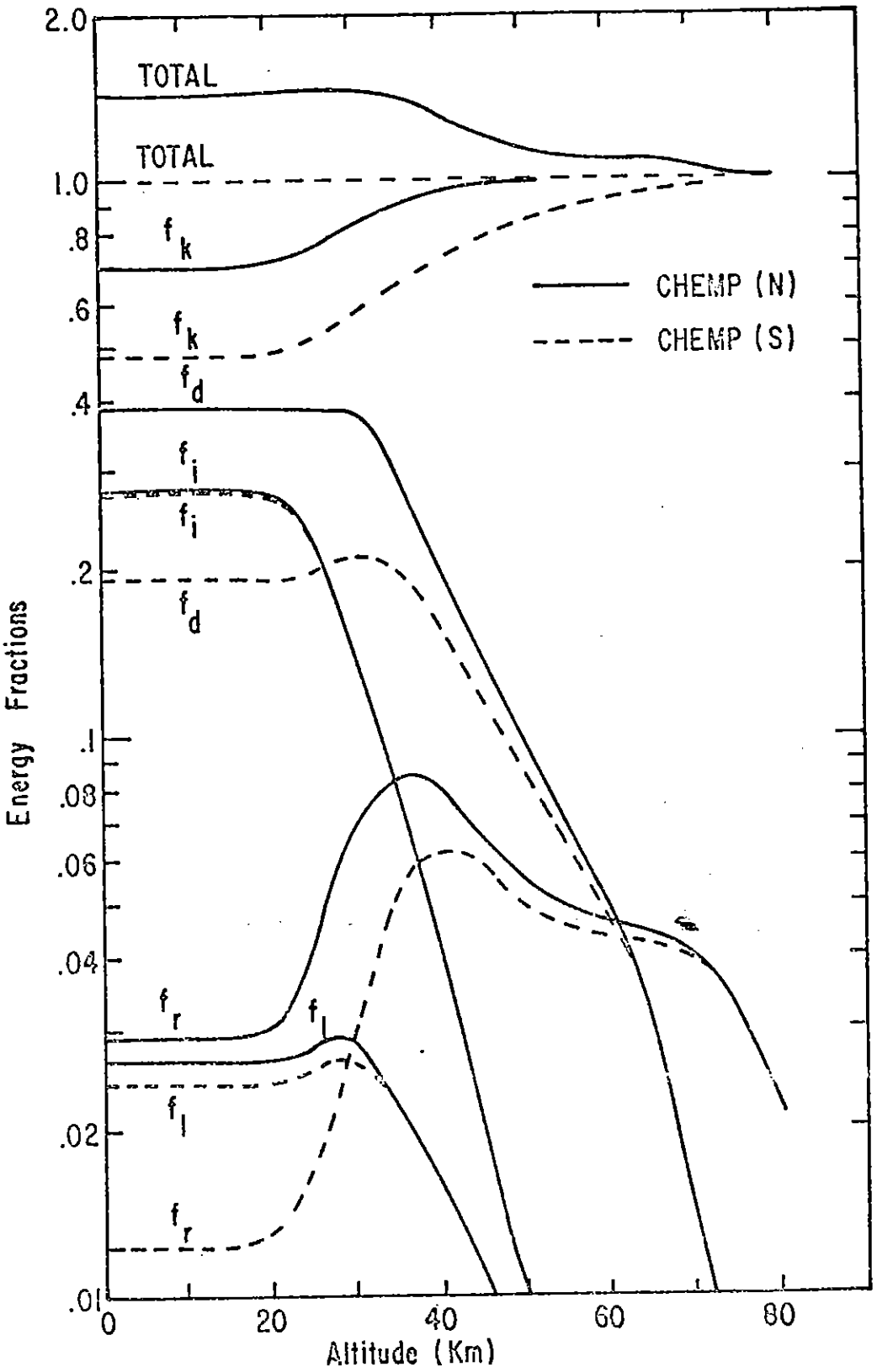

Figure 5. Energy Fractions at 5.8×10^{-8} sec

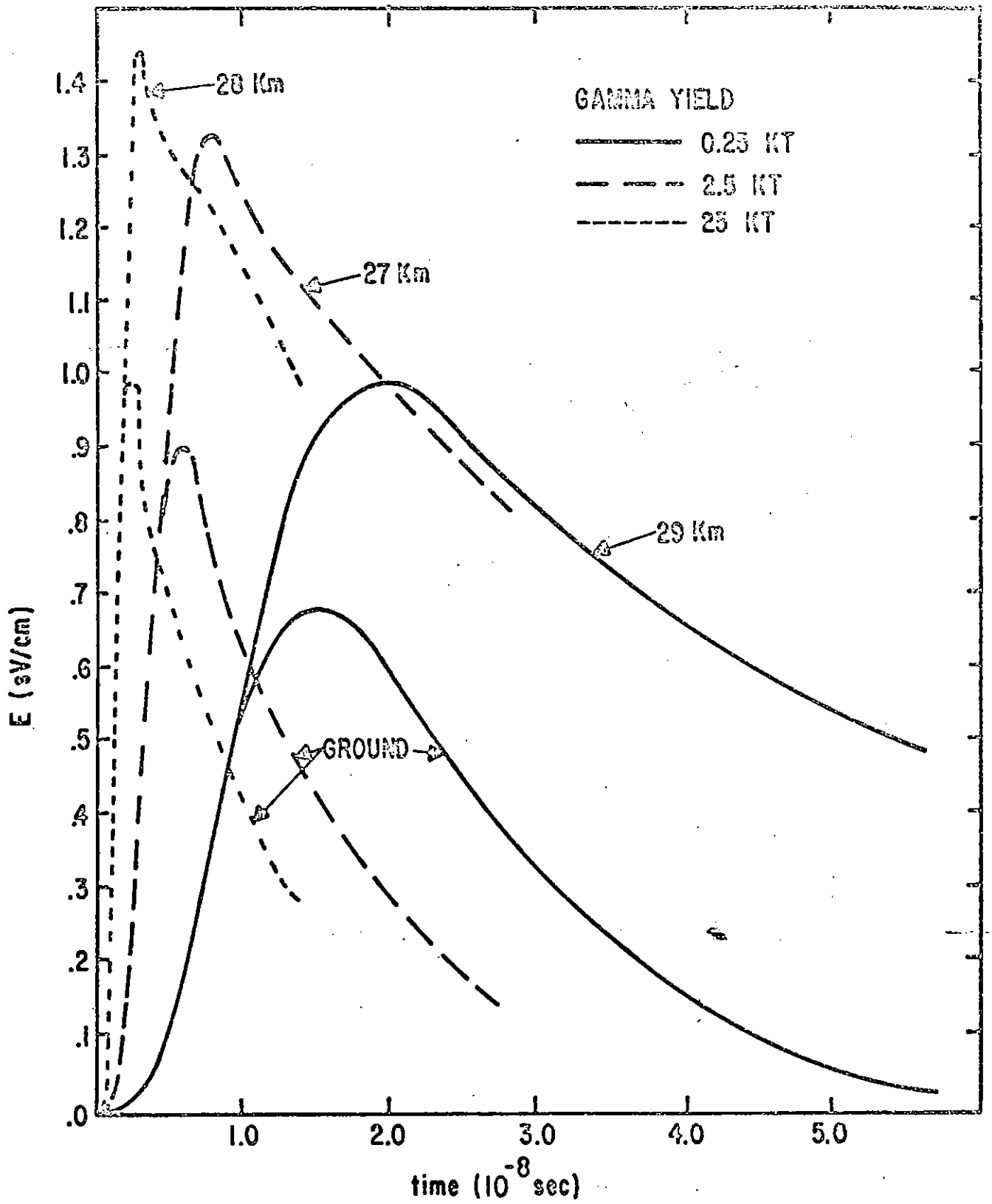

Figure 6. Pulse Shape as a Function of Yield Directly Below Burst at 100 km Assuming a 1.5 MeV Gamma Source

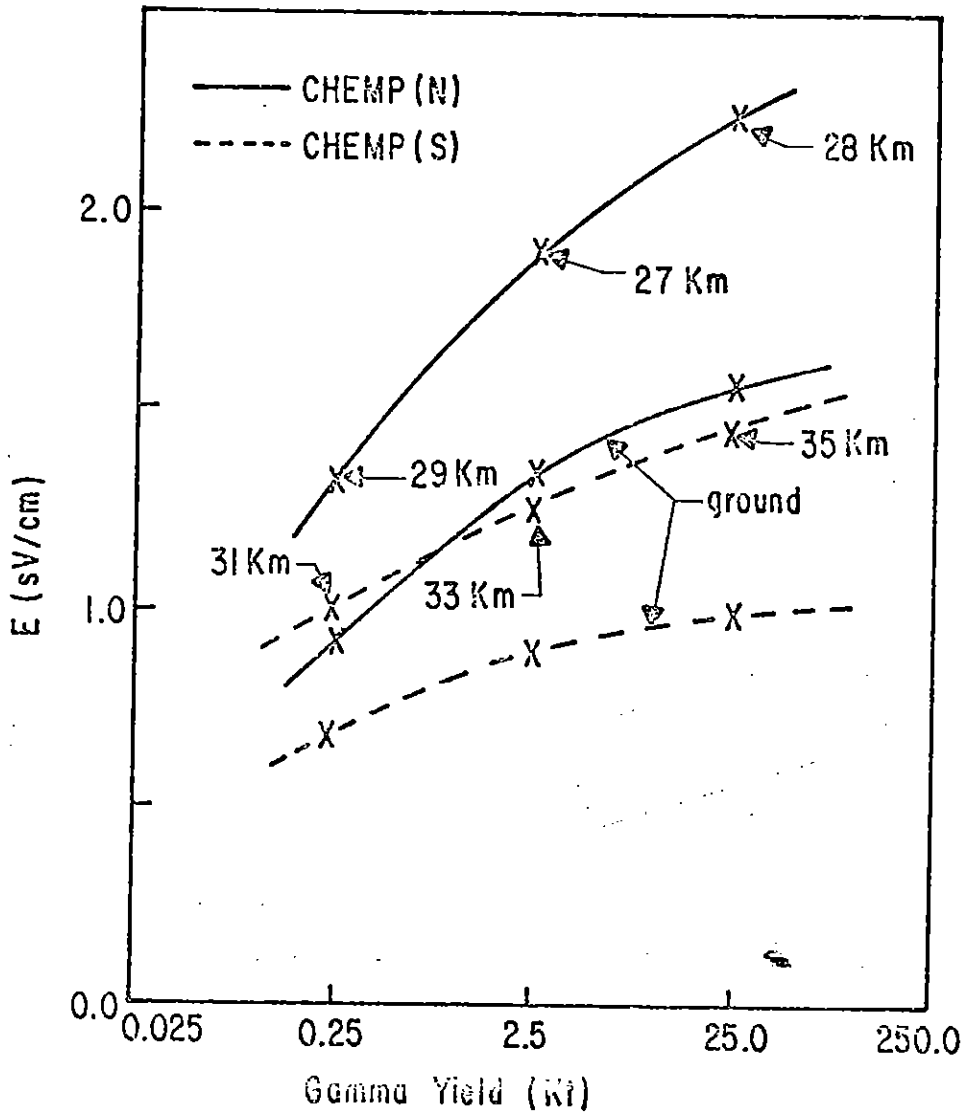

Figure 7. Maximum Fields Directly Below a 100 km Burst of 1.5 MeV Gammas as a Function of Yield

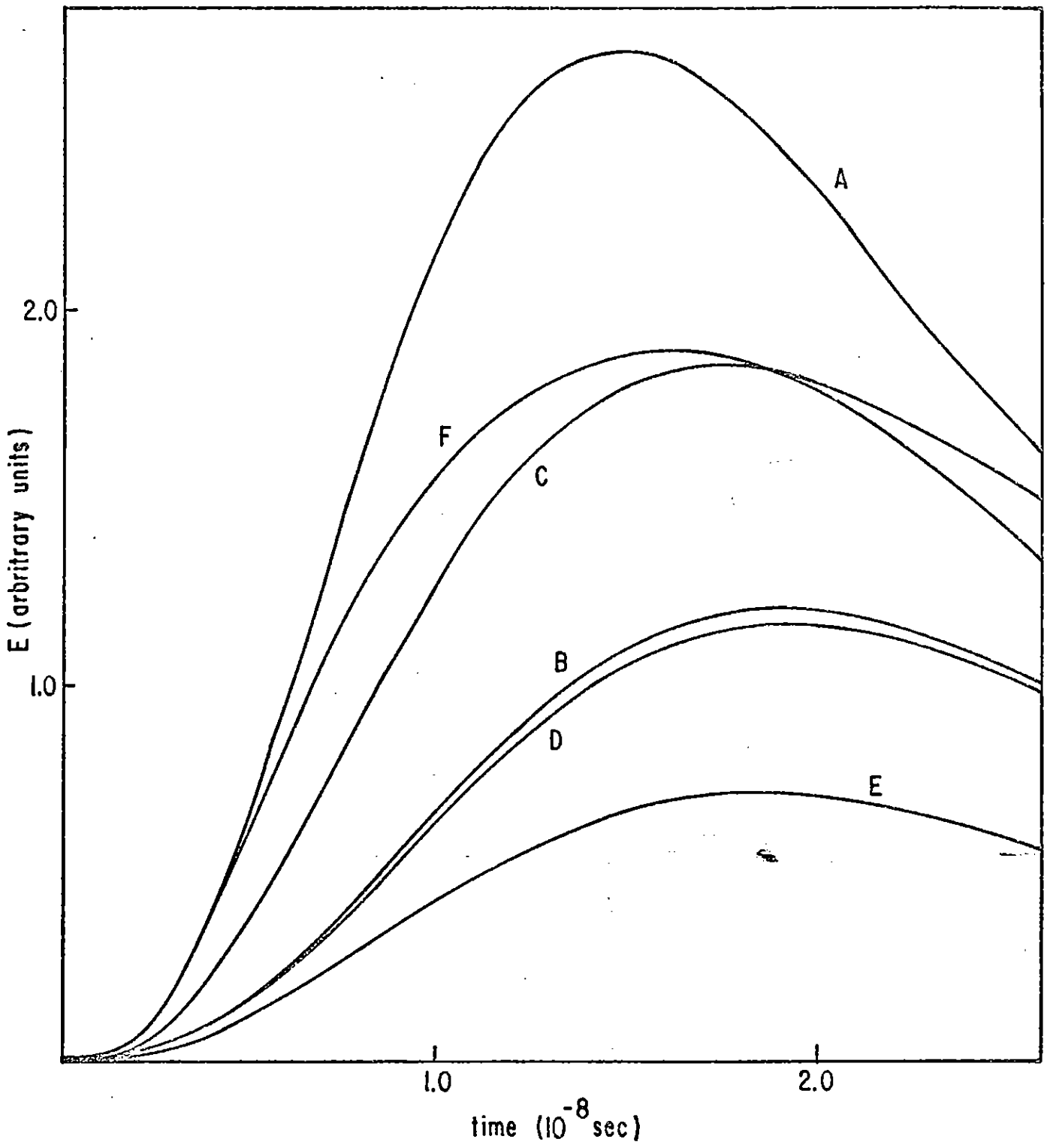

Figure 8. Effects of Various Source Approximations

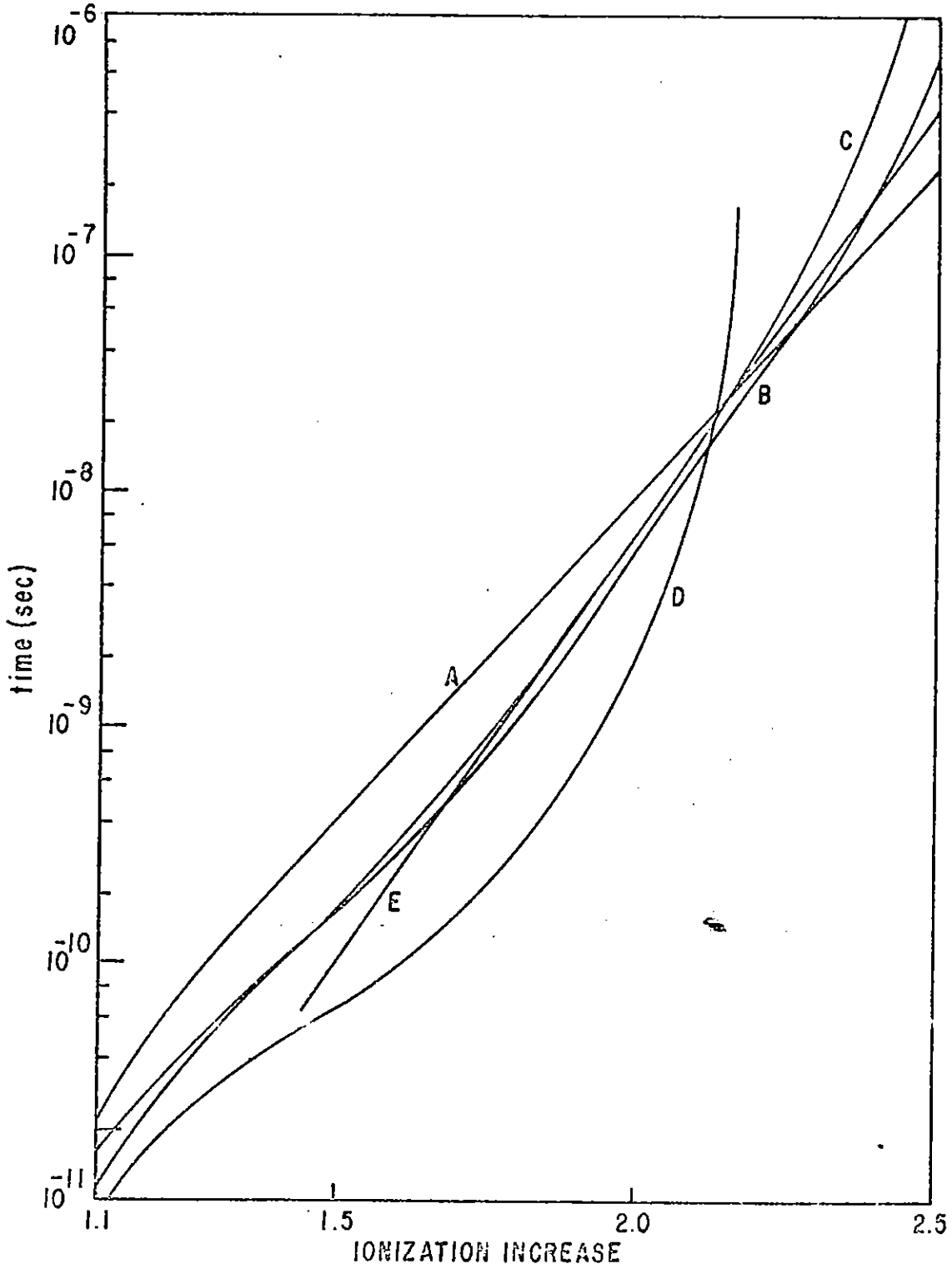

Figure 9. Ionization Lag Models

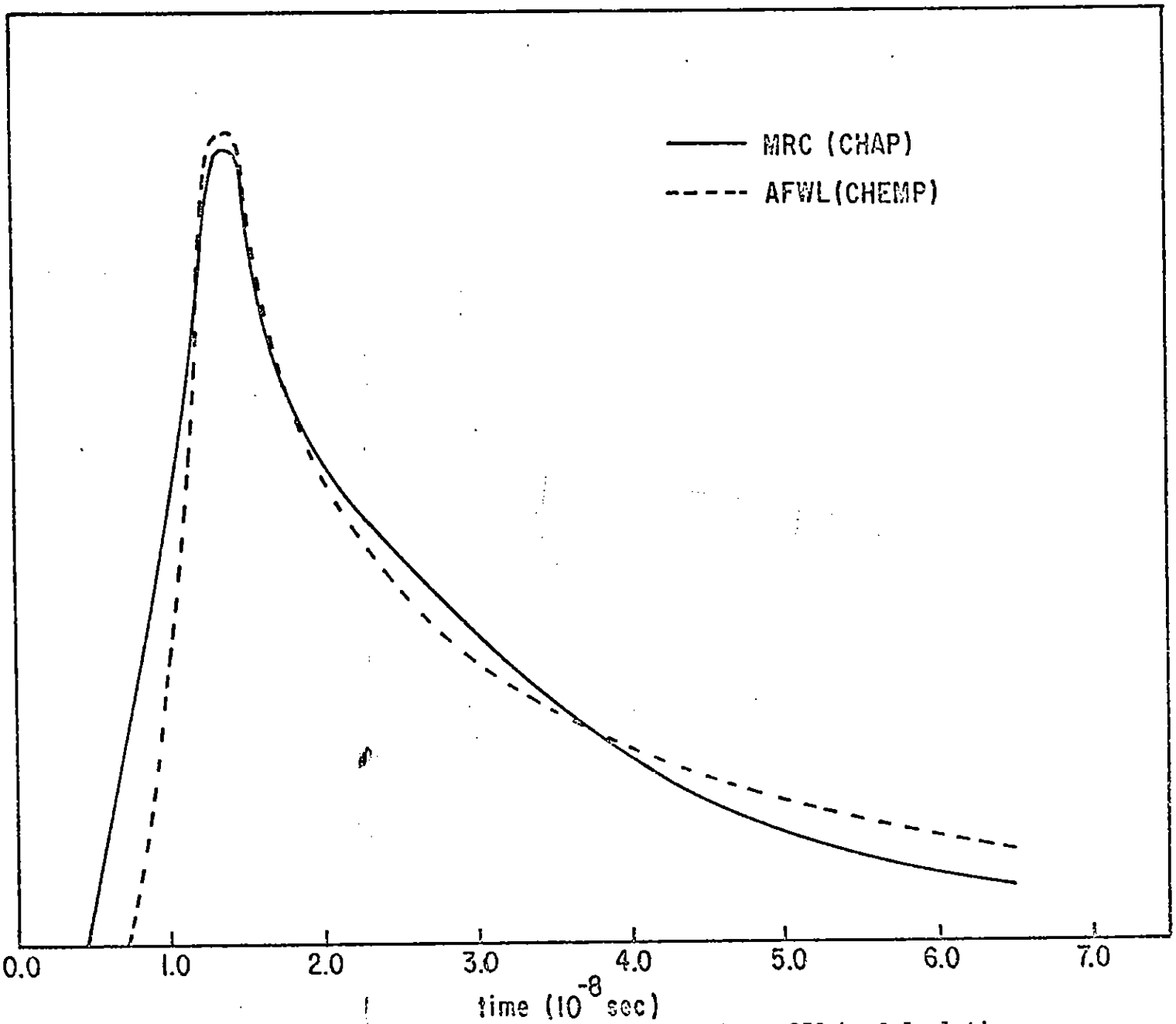

Figure 10. Comparison of MRC and AFWL 25 KTγ at 250 km Calculations

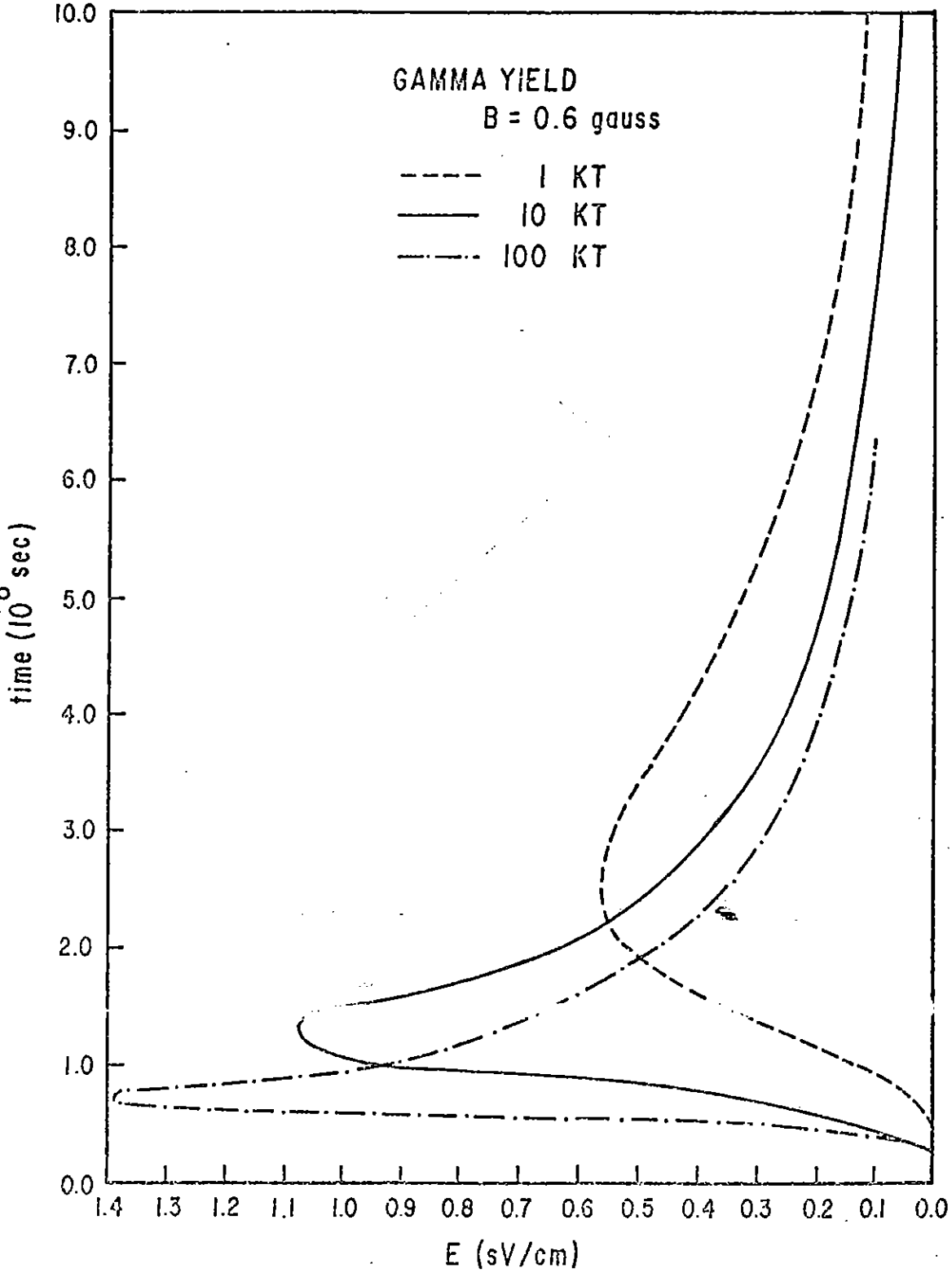

Figure 11. Comparison of Fields from 1-, 10-, and 100-KT Gamma Yields at 250 km

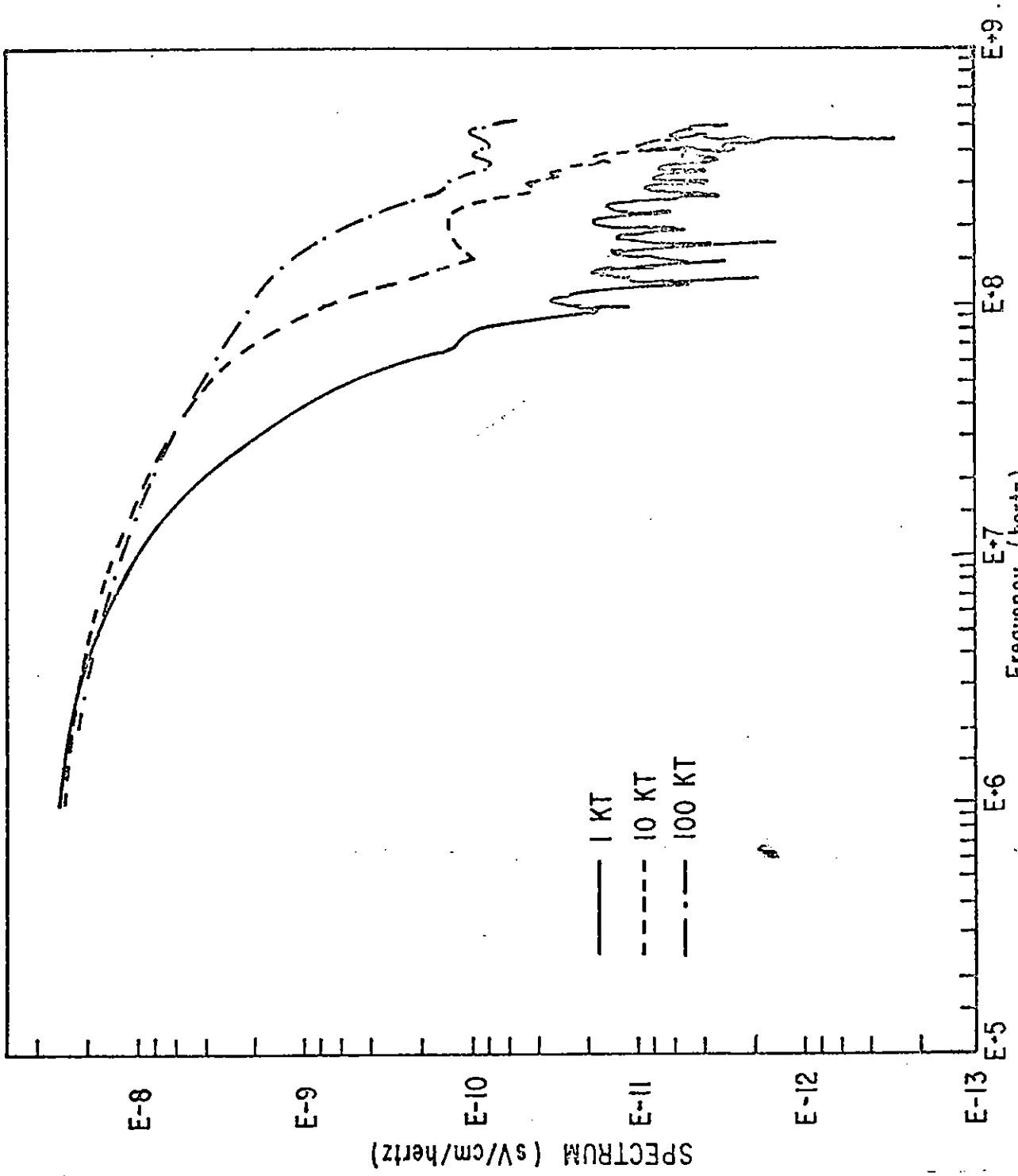

Figure 12. Fourier Transforms of Fields Shown in Figure 11

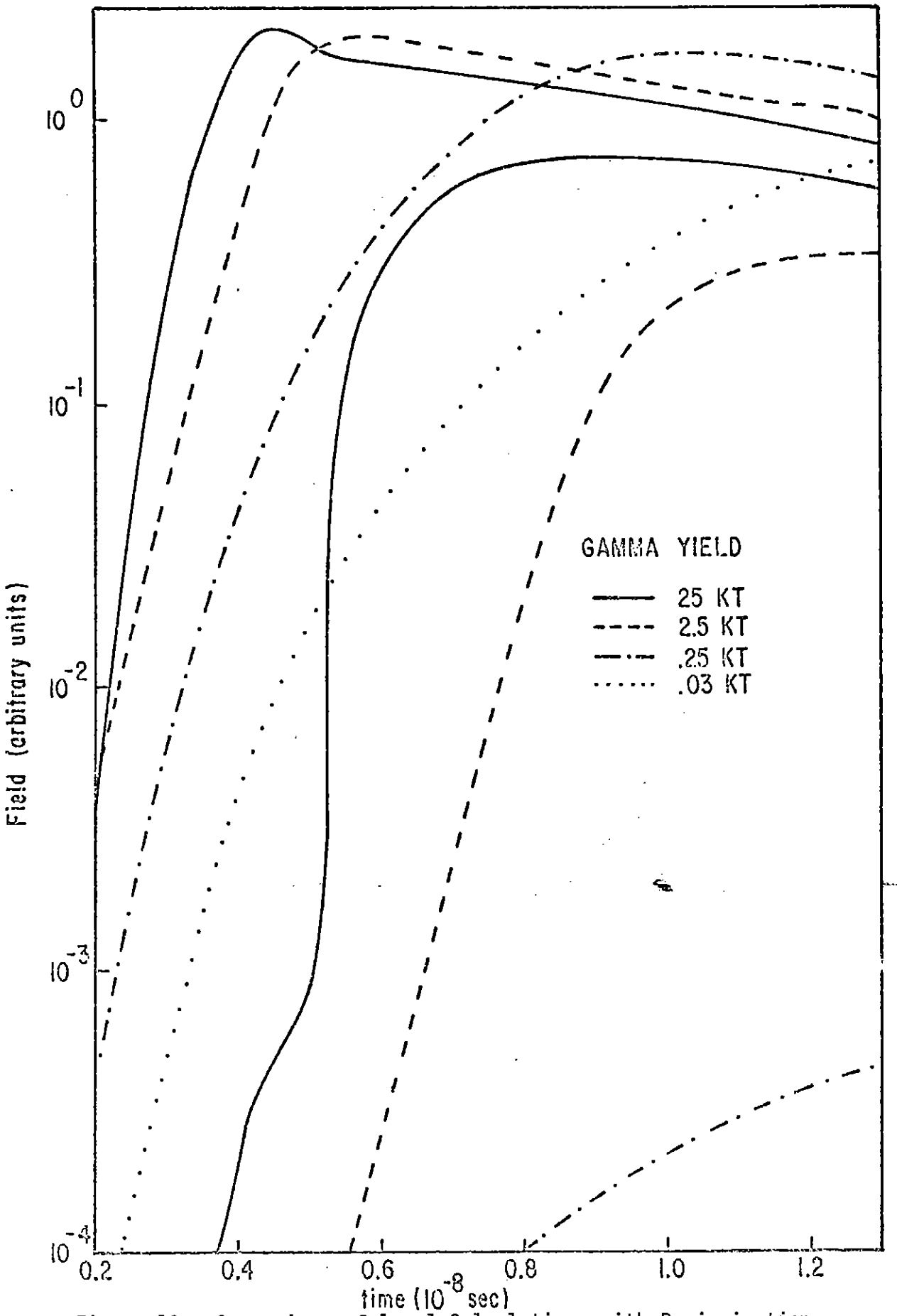

Figure 13. Comparison of 1 x 1 Calculations with Preionization and Vertical Line of Sight

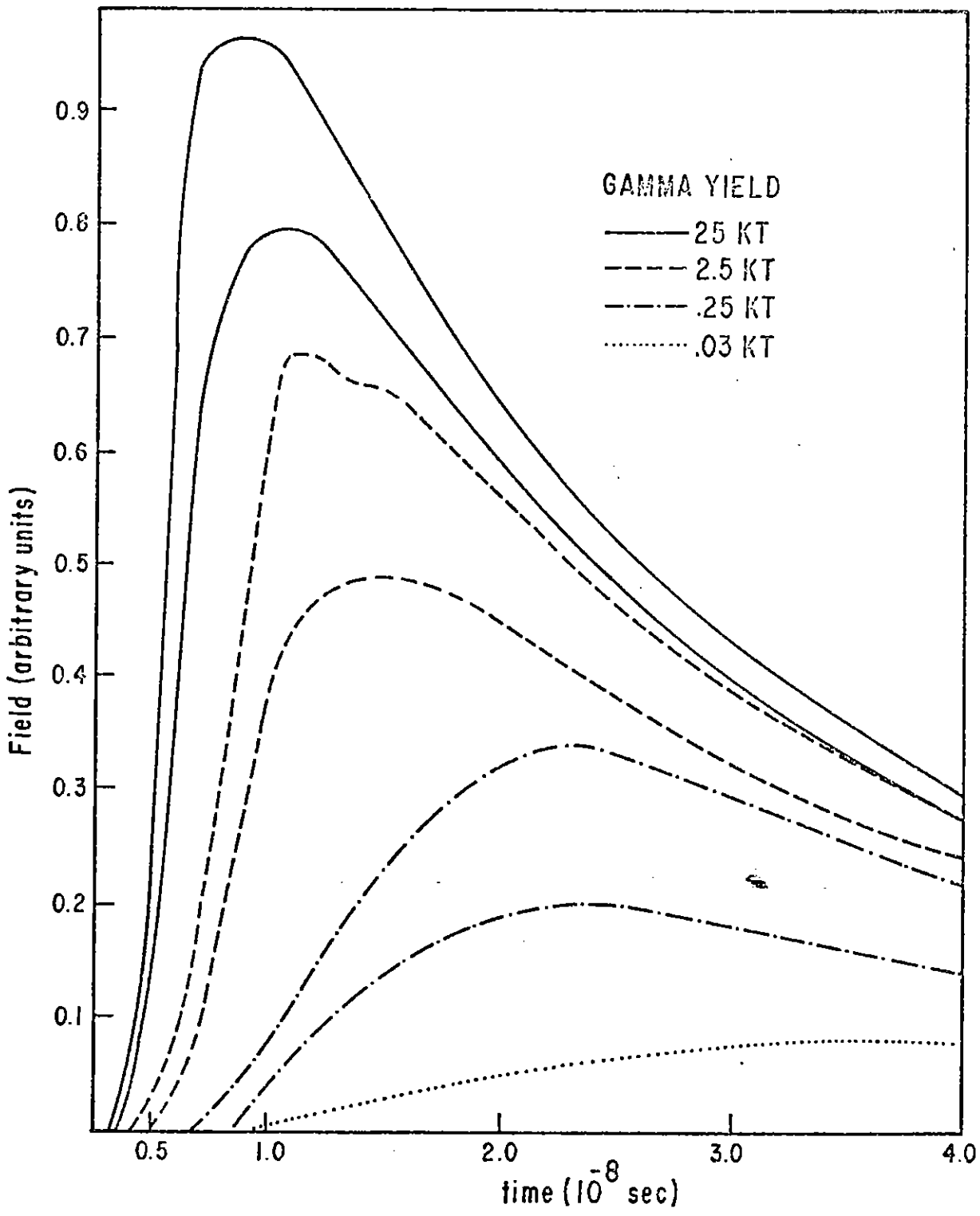

Figure 14. Comparison of 1 x 1 Calculations with Preionization and Line of Sight to the Horizon

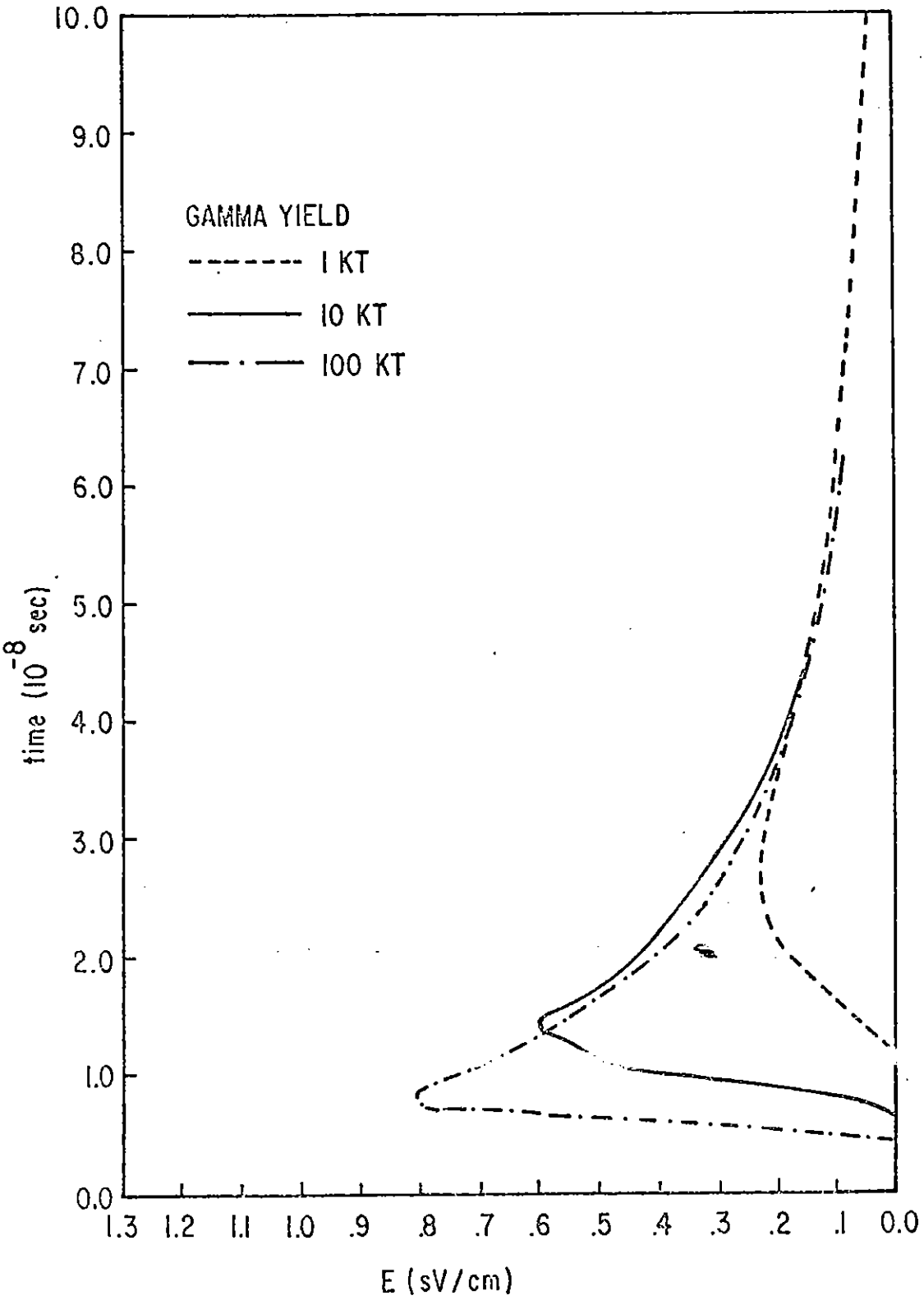

Figure 15. Comparison of 4 x 4 Calculations with Preionization

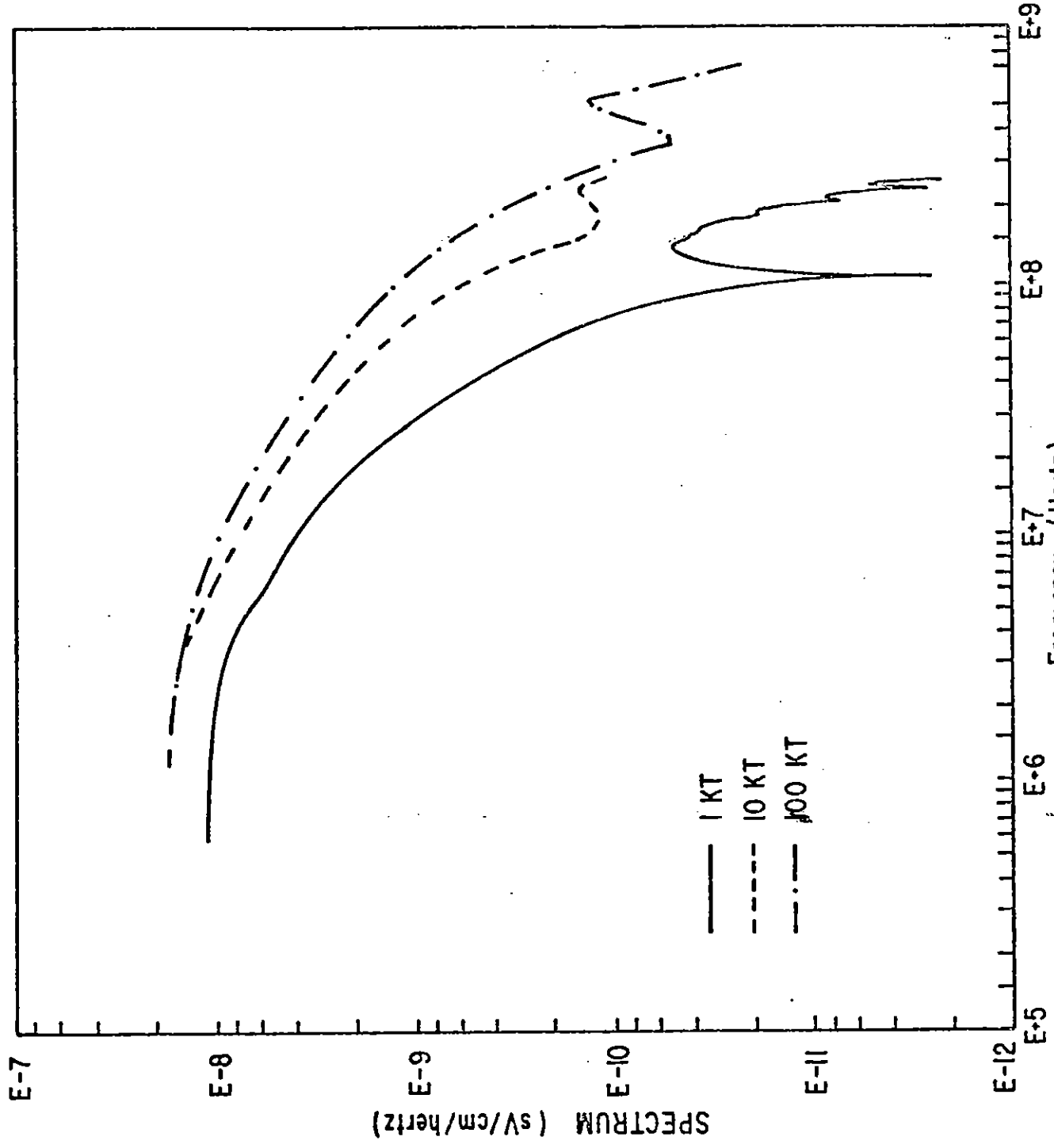

Figure 16. Fourier Transforms of Fields Shown in Figure 15

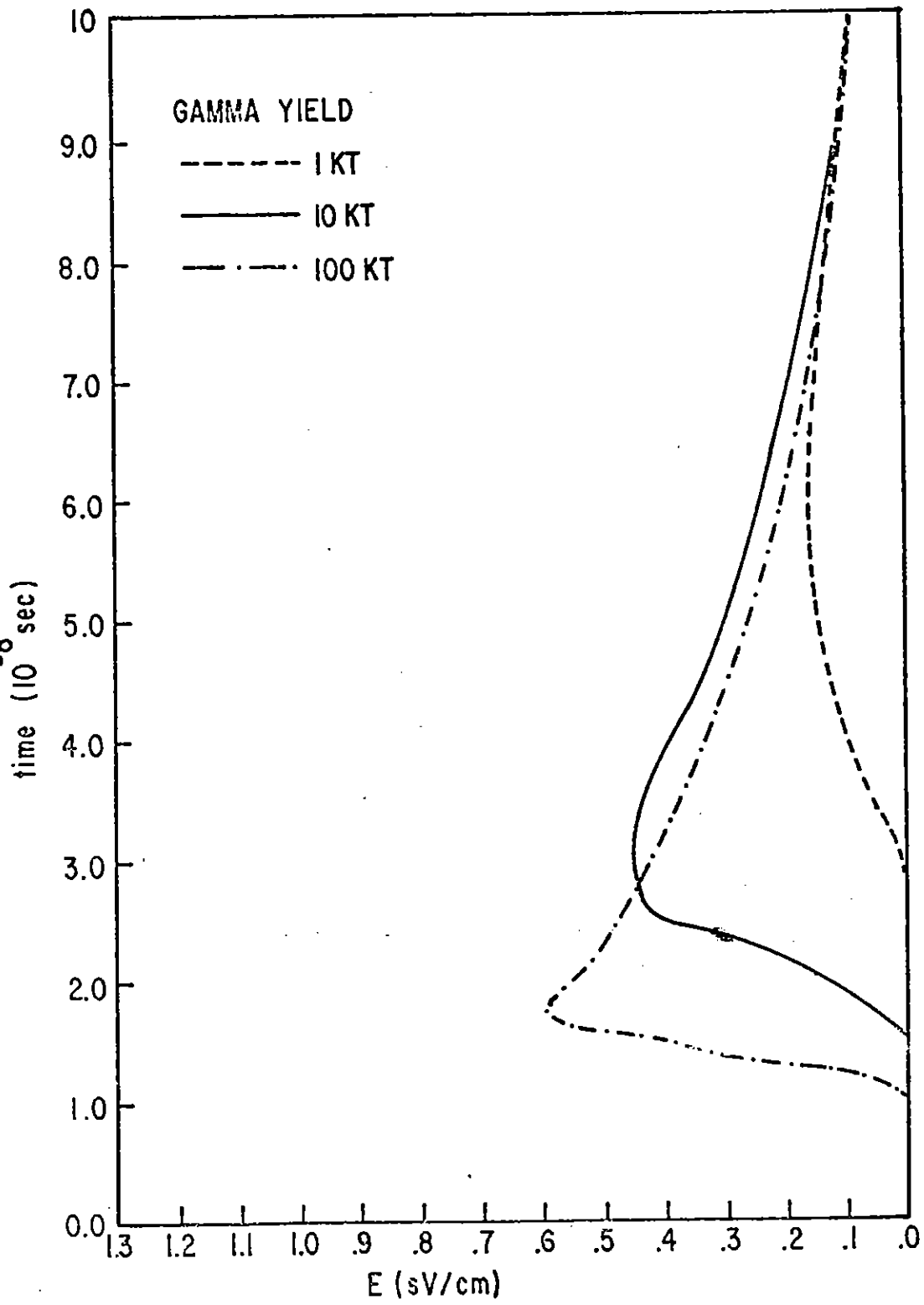

Figure 17. Comparison of 4 x 4 Calculations with Preionization and Long Gamma Pulse

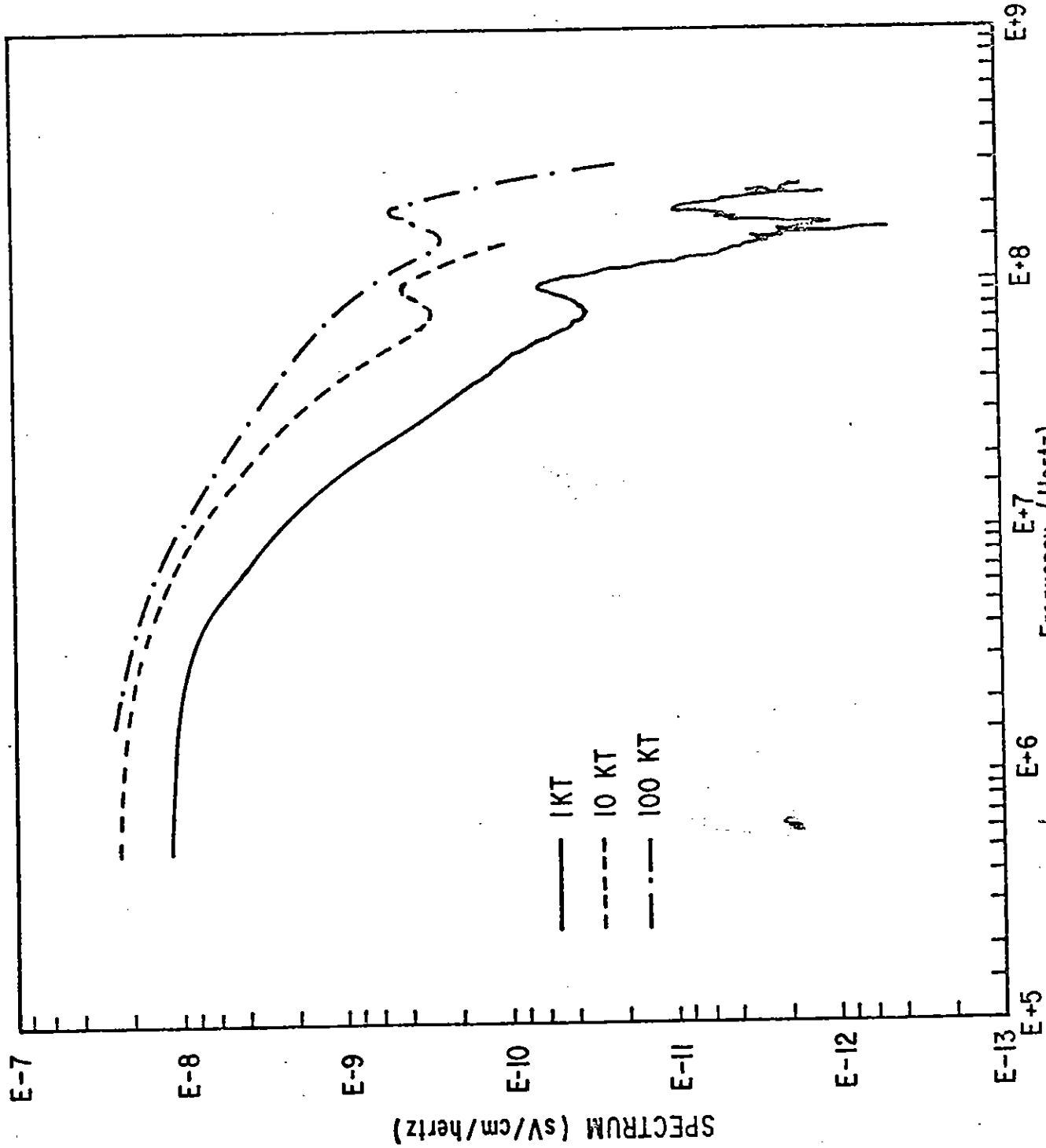

Figure 18. Fourier Transforms of Fields Shown in Figure 17

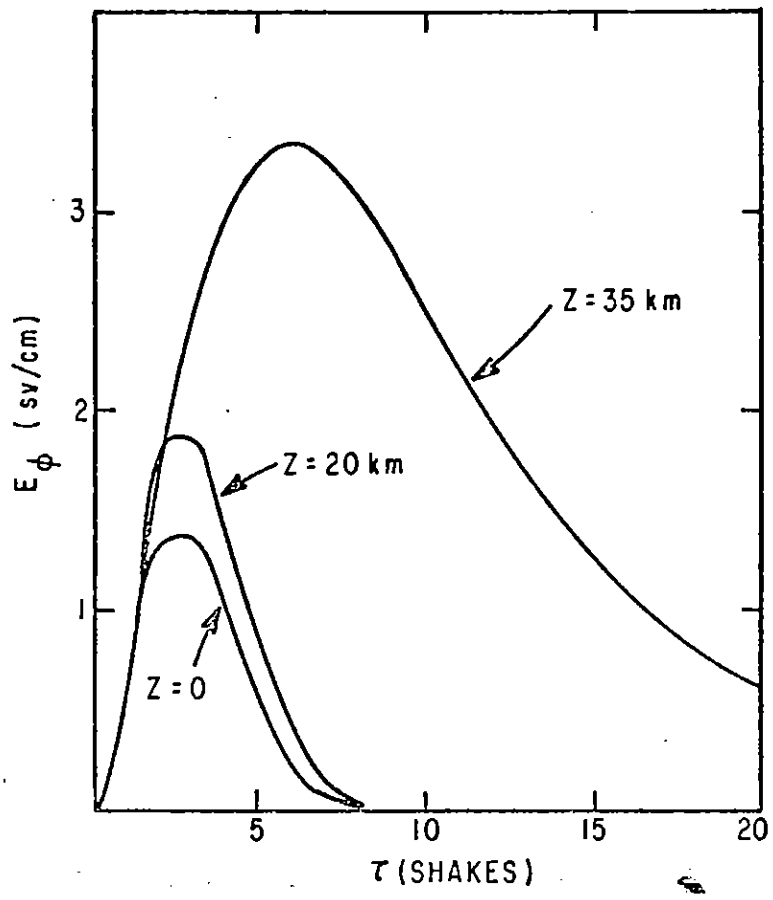

Figure 19. The EMP Waveform at 35-, 20-, and 0-km Altitudes Generated by a 10^{19} erg Monoenergetic (1.5 MeV Gamma Source at 100 km)

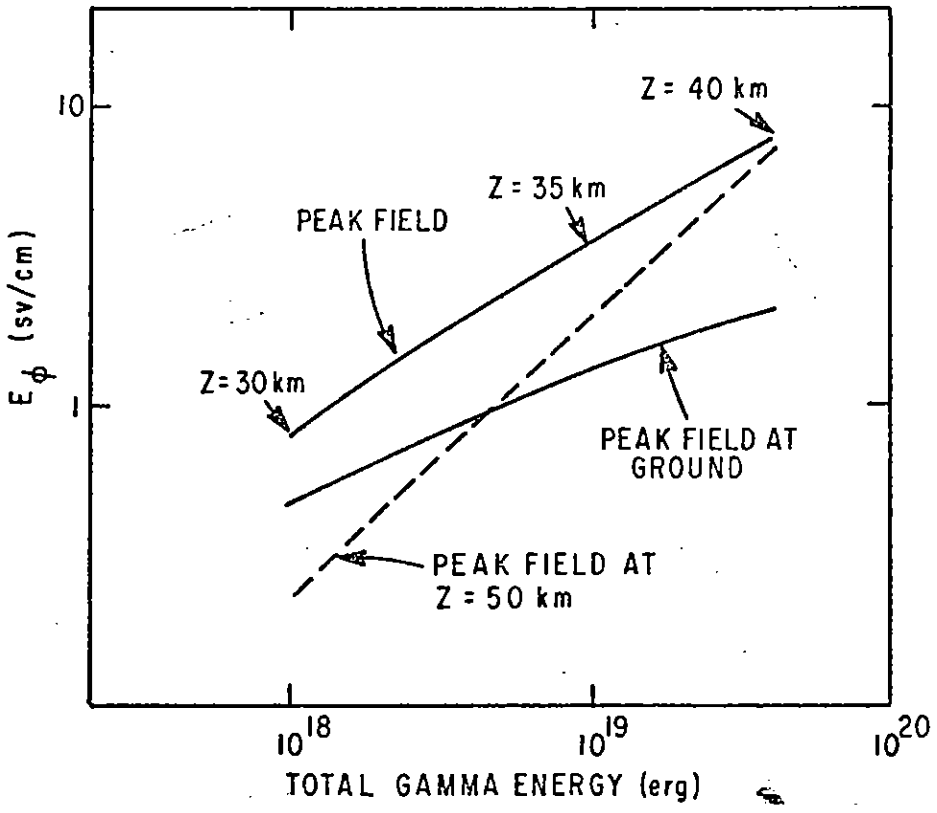

Figure 20. The Maximum Propagating Electric Field and the Field Observed at the Surface of the Earth as a Function of Gamma Source Energy

REFERENCES

1. Erkkila, J.H., Calculation of the EMP from High Altitude Nuclear Detonations, EMP Theoretical Note 26, April 1967.

2. Wittwer, L.A., Brau, J.E., and Canavan, G.H., CHEMP: A Code for Self-Consistent Calculations of High-Altitude EMP, Theoretical Note, March 1974.

3. Crain, C.M., Private Communication.

4. Longley, H.J. and Longmire, C.L., Results from CHAP-1971, Environment Note 19, January 1972.

5. Longley, H.J. and Longmire, C.L., Development of the CHAP EMP Code, (U), Theoretical Note 185, January 1972 (Conf).

6. Karzas, W.J., Comments on Booker's Consideration of the Effect of Atmospheric Scattering on the Electromagnetic Radiation by Compton Electrons, RDA Working Note, 21 August 1973.

7. Knutson, G.B., The Effect of Nuclear-Colomb Electron Scattering on High Altitude EMP Sources, EMP Theoretical Note 161, February 1972.

8. Wittwer, L.A., Brau, J.E., and Canavan, G.H., Effects of Nuclear Scattering and Energy Loss on Small Signal High-Altitude EMP Calculations, Theoretical Note 191, January 1974.

9. Karzas, W.J. and Latter, R.A., Detection of the Electromagnetic Radiation from Nuclear Explosions in Space, Theoretical Note 40, October 1964.

10. Crain, C.M., A Numerical Example of the Effect of Atmospheric Scattering on Predicted EMP Environments, RAND Working Note, 30 July 1973.

11. Longmire, C.L. and Longley, H.J., Improvements in the Treatment of Compton Current and Air Conductivity in EMP Problems, Theoretical Note 128.

12. Longmire, C.L., Developments in EMP Theories, Mission Research Corporation, Invited paper at the Joint EMP Technical Meeting, Air Force Weapons Laboratory, Kirtland AFB, NM, 25-27 September 1973.

13. Lunn, P.W., Private Communication.

14. Higgins, D. F., Longmire, C. L., and O'Dell, A.A., A Method for Estimating the X-Ray Produced Electromagnetic Pulse Observed in the Source Region of a High Altitude Burst, Theoretical Note 181, February 1973.